The di-iron RIC (YtfE) protein of *Escherichia coli* interacts with the DNA-binding protein from starved cells (Dps) to diminish RIC-protein-mediated redox stress

Liliana S. O. Silva[1], Joana M. Baptista[1], Charlotte Bately[2], Simon C. Andrews[2], and Lígia M Saraiva[1,*]

[1]Instituto de Tecnologia Química e Biológica NOVA, Av. da República, 2780-157 Oeiras, Portugal

[2] School of Biological Sciences, Knight Building, University of Reading, Reading RG6 6AJ, UK

*Corresponding author:

Lígia M. Saraiva

Av. da República, 2780-157 Oeiras, Portugal

Phone: +351-214469328; Fax: +351-214411277

E-mail: lst@itqb.unl.pt

Abstract

The RIC (Repair of Iron Clusters) protein of *Escherichia coli* is a di-iron hemerythrin-like protein that has a proposed function in repairing stress-damaged iron-sulphur clusters. In this work, we performed a Bacterial Two Hybrid screening to search for RIC-protein interaction partners in *E. coli*. As a result, the DNA-binding protein from starved cells (Dps) was identified and its potential interaction with RIC was tested by BACTH, Bimolecular-Fluorescence-Complementation and pull-down assays. Using the activity of two Fe-S-containing enzyme as indicators of cellular Fe-S cluster damage, we observed that strains with single deletions of *ric* or *dps* have significantly lower aconitase and fumarase activities. In contrast, the double *ric dps* mutant strain displayed no loss of aconitase and fumarase activity with respect to the wild type. Additionally, while complementation of the *ric dps* double mutant with *ric* led to a severe loss of aconitase activity, this effect was no longer observed when a gene encoding a di-iron site variant of the RIC protein was employed. The *dps* mutant exhibited a large increase in ROS levels, but this increase was eliminated when *ric* was also inactivated. Absence of other iron-storage proteins, or of peroxidase and catalases, had no impact on RIC-mediated redox stress induction. Hence, we show that RIC interacts with Dps in a manner that serves to protect *E. coli* from RIC-protein-induced ROS.

Importance

The mammalian immune system produces reactive oxygen and nitrogen species that kill bacterial pathogens by damaging key cellular components such as lipids, DNA and proteins. However, bacteria possess detoxifying and repair systems that mitigate these deleterious effects. The *E. coli* RIC (Repair of Iron Clusters) protein is a di-iron hemerythrin-like protein that repairs stress-damaged iron-sulphur clusters. *E. coli* Dps is an iron-storage protein of the ferritin superfamily with DNA-binding capacity that protects cells from oxidative stress. This work shows that the *E. coli* RIC and Dps proteins interact in a fashion that counters RIC-protein-induced ROS. Altogether, we provide evidence for the formation of a new bacterial protein complex and reveal a novel contribution for Dps in bacterial redox-stress protection.

Keywords

E. coli, di-iron RIC protein, YtfE, Dps, oxidative stress, nitrosative stress

Running Title

Di-iron RIC protein interacts with Dps

Introduction

During the infection process, bacterial pathogens are able to survive aggressive environments through the activation of specific stress-resistance genes. One such example of a stress-induced gene is *ric*. This gene encodes the 'Repair of Iron Centre' (RIC) protein that contains a di-iron centre and contributes to the protection of bacterial pathogens such as *Escherichia coli*, *Haemophilus influenzae*, *Salmonella* spp., *Yersinia* spp. and *Clostridium* spp. during exposure to nitrosative and/or oxidative stress (1). The *ric* gene is induced upon exposure to either oxidative or nitrosative stress, and in *E. coli*, *Staphylococcus aureus, Neisseria gonorrhoeae, H. influenza* and *Cryptococcus neoformans* the RIC protein is thought to confer stress resistance through maintenance of the activity of various Fe-S containing enzymes (1–3). Such an effect is well demonstrated for *E. coli* and *S. aureus* where RIC proteins restore the activity of oxidatively and nitrosatively-damaged Fe-S clusters in the TCA cycle enzymes, aconitase and fumarase (1, 4, 5) In *E. coli*, the RIC protein also acts under non-stress conditions to maintain aconitase and fumarase activities (6). Further, the *E. coli* RIC protein delivers iron (most likely in the ferrous state) for the assembly of Fe-S clusters in spinach apo-ferredoxin and in the *E. coli* Fe-S cluster-assembly scaffold protein, IscU (7). The RIC protein also contributes to the survival of *S. aureus* and *H. influenzae* in activated macrophages, and is required for full virulence in *S. aureus* when infecting the wax moth larva infection-model, *Galleria mellonella* (3, 8). Thus, the RIC protein has an apparent role in bacterial pathogenicity through mediation of Fe-S cluster stability during exposure to redox- and/or nitrosative-stress.

The RIC proteins of *E. coli* and *S. aureus* contain di-iron centres of the histidine/carboxylate type within a four-helix-bundle fold (9). The UV-visible spectrum of

oxidized RIC protein exhibits a broad band at *ca.* 350 nm and Electron Paramagnetic Resonance (EPR) spectroscopy indicates that the principal g-values are below 2 (g=1.96, 1.92 and 1.88), which is indicative of a S=½ spin state in a mixed valence and anti-ferromagnetically coupled Fe(III)-Fe(II) binuclear iron centre. Mössbauer spectroscopy showed that the mixed-valence Fe(III)–Fe(II) di-iron centre of the RIC protein is more labile than that of the μ(oxo)-diferric form (7).

RIC proteins possess several highly-conserved amino acid residues of which some have been shown to influence the properties of the di-iron centre and/or function of the protein. In particular, substitution of residues His129, Glu133 or Glu208 of the *E. coli* RIC protein abrogated its ability to protect the Fe-S cluster of aconitase. Moreover, two μ-carboxylate bridges contributed by Glu133 and Glu208, linking the two di-iron site atoms, were shown to be required for the assembly of a stable di-iron centre (10). These studies also demonstrated the important contribution of the conserved His84, His129, His160, His204, Glu133 and Glu208 residues in ligating the di-iron centre within the four-helix bundle fold, and these di-iron coordination roles were recently confirmed by X-ray crystallographic structural studies (11).

In the work reported here, we sought to identify proteins that interact with, and support the function of, the RIC protein of *E. coli*. For this purpose, an *E. coli* library was screened for RIC protein interaction partners using the Bacterial Adenylate Cyclase Two Hybrid system (BACTH). Potential interacting gene products were further tested by BACTH, Bimolecular Fluorescence Complementation (BiFC) and pull-down assays. Our protein-protein interaction studies revealed that the RIC protein interacts with the DNA-binding protein

from starved cells (Dps). Dps is a symmetrical dodecameric iron-storage protein of the ferritin superfamily that contains a di-iron ferroxidation centre located at the interface between subunits (12–14). Dps sequesters ferrous iron, which is oxidized preferentially by hydrogen peroxide at its di-iron centre and then deposited for storage as Fe(III) oxyhydroxide in the central cavity as an iron core; the sequestered iron can subsequently be released by reduction (14, 15). The ferroxidase activity, DNA-binding and iron-sequestration properties of Dps confer cells with protection from oxidative stress and nutrient deprivation, as judged by the reduced survival of *dps* mutants under stress conditions including starvation, oxidative stress, metal toxicity, and thermal stress (16). The physiological relevance of the interaction between the RIC protein and Dps was examined and the results revealed that Dps modulates the function of RIC.

Results

Identification of novel potential RIC-protein-interaction partners by screening a bacterial two-hybrid *E. coli* library

We used a genetic approach to further assess the physiological role of RIC in *E. coli*, by employing the bacterial two-hybrid (BACTH) system (17) to screen the *E. coli* genome for gene products that could interact with RIC. For this purpose, RIC was fused to the C-terminus of the *B. pertussis* adenylate cyclase T25 fragment and used as 'bait' to screen previously constructed partial-*Sau*3A-digested *E. coli* DNA random libraries that express fusions to the N-terminus of the *B. pertussis* adenylate cyclase T18 fragment (18). We isolated 22 positive recombinant Lac^+ colonies, from which plasmids were purified and then transformed into *E. coli* DHM1 harbouring pKT25-RIC, or the empty vector pKT25 (negative control), or pKT25-TorD (false positive control), followed by the determination of the β-galactosidase specific activities (Figure 1). Seven pKT25-RIC transformants, harbouring plasmids A to G, exhibited significant β-galactosidase activity indicative of a specific interaction (Figure 1). Nucleotide sequencing followed by BLAST analysis was used to identify the genes within the inserts of these plasmids. Sequencing data revealed that plasmids A to C contain an ~2 kb *E. coli* DNA fragment upstream of the T18 Cya domain, and that all cases included the complete *efp* and *ecnA* genes, and part of the *ecnB* gene. The *efp* gene encodes the elongation factor EF-P, a translation factor that facilitates the *in vitro* the formation of the first peptide bond during translation (19, 20). The gene

cluster *ecnAB* expresses two small cell-membrane associated entericidin lipoproteins, forming EcnAB a toxin-antitoxin module that regulates a programmed bacterial cell death under high osmolarity conditions, with EcnA acting as the antidote for the bacteriolytic entericidin, EcnB (21).

The other four plasmids D to G also contained a ~2 kb insert located upstream of the T18 Cya domain, but in these cases the inserts carried the entire *rhtA* gene, encoding an inner-membrane transporter involved in resistance to homoserine/threonine (22), and the *dps* gene, encoding the DNA-binding and iron-storage protein from *s*tarved cells (12). Like RIC, *E. coli* Dps has been implicated in oxidative-stress protection, which raises the possibility of a functional association between these two proteins that might be dependent on their direct interaction. For this reason, the potential interaction between the two proteins was investigated further in order to establish its validity and determine its physiological purpose.

E. coli RIC protein interacts with Dps

To determine whether the interaction between the RIC protein and Dps, as identified through the screening of the pUT18 library, is indeed genuine, further BACTH experiments were performed. To enable such experiments, the gene encoding the RIC protein was cloned into pUT18C and pUT18 vectors (to create T18-RIC and RIC-T18 fusions), and the *dps*-coding region was introduced into the pKNT25 vector (to give Dps-T25 fusions), following which the β-galactosidase activities of the corresponding co-transformants were measured. High β-galactosidase activities were recorded for both sets of the RIC-Dps

BATCH combinations tested, with activities 4-6 times greater than those of the controls (Figure 2A), indicative of interaction between the RIC protein and Dps within the cytosol of *E. coli*.

A second approach was used to test the proposed RIC-Dps interaction, which involved a Bimolecular Fluorescence Complementation (BiFC) assay. In this method, one of the two proteins of interest is fused to the N-terminal half of the green fluorescent protein (GFP), and the other protein of interest is fused to the C-terminal half; the assay depends upon an interaction between the two proteins that promotes the reassembly of the two halves of GFP such that emission of fluorescence is restored (23). Thus, GFP fusions (both the N- and C-terminal domains) were generated for both the RIC protein and Dps, and the fluorescence intensity of the corresponding *E. coli* cells containing plasmids co-expressing the RIC and Dps fusions was measured (Figure 2BC). The data showed that cells expressing $RIC^{C\text{-}GFP}$ and $Dps^{N\text{-}GFP}$ exhibit an approximately six-fold higher fluorescence relative to the control, although transformants expressing $RIC^{N\text{-}GFP}$ and $Dps^{C\text{-}GFP}$ presented fluorescence levels similar to that of the control samples.

The RIC protein consists of two domains: a short N-terminal 'ScdA_N' domain of ~60 residues of unclear function with a highly-conserved pair of Cys residues (11); and a larger C-terminal 'hemerythrin' domain of ~140 residues that forms a di-iron centre. We tested the BiFC interaction between Dps and a truncated form of RIC that lacks the so-called first Scd_N domain to determine which of the two RIC protein domains is responsible for the observed interaction with Dps. The results showed that the degree of interaction between the truncated RIC protein and Dps is similar to that observed when using the full-length protein (Figure 2C). Thus, the interaction observed here between the RIC protein and Dps appears to be mediated through the C-terminal hemerythrin domain of the RIC protein.

The interaction between RIC and Dps was also investigated by a pull-down assay. To this end, cells containing plasmids that express non-labelled Dps and N-terminally His-tagged-RIC were treated with formaldehyde, as described in Methods, to promote *in vivo* cross-linking. The cell extract was loaded into a Ni-chelating column and the His-Tag RIC was eluted at 100 mM of imidazole buffer. The fraction was analysed by denaturing SDS-PAGE, and Western blotting in which the *E. coli* Dps antibody was used. Also, cells expressing only the non-labelled Dps were treated and analysed similarly to serve as control. The results depicted in Figure 2D show that elution of His-Tag RIC occurred together with a band that has a molecular mass correspondent to that of Dps. This band was proved by Western-blotting to be the *E. coli* Dps (Figure 2D). Therefore, the pull-down assays support the interaction between RIC and Dps**.**

Dps modulates the function of the RIC protein in maintaining Fe-S cluster status

The RIC protein has been linked to the resistance of *E. coli* to oxidative and nitrosative stresses as its inactivation decreases the survival of *E. coli* upon exposure to hydrogen peroxide or nitric oxide donors (4). Due to the interaction of the RIC and Dps proteins shown above, we questioned whether Dps could contribute to the stress protection afforded by the RIC protein. To test this possibility, a Δ*dps*Δ*ric* double mutant was constructed and the growth of *E. coli* wild type, Δ*ric*, Δ*dps*, Δ*dps*Δ*ric* mutants under oxidative and nitrosative stress conditions was tested (Figure 3). The growth experiments showed that inactivation of *ric* resulted in impaired growth under stress conditions imposed by 4 mM H_2O_2 or 250 μM spermine NONOate (Figure 3), which is consistent with previous reports

(4). However, the *dps* mutation had little impact on growth under these conditions. Combining the Δ*dps* mutation with the Δ*ric* mutation did not result in any further growth reduction under the same stress conditions, i.e. the Δ*dps*Δ*ric* strain grew similarly to the Δ*ric* strain under the oxidative and nitrosative stress conditions employed (Figure 3). Thus, Dps does not notably compensate for the lack of the RIC protein under peroxide or NO-induced stress.

Another characteristic of the *E. coli ric* mutant is the reduced endogenous activity of Fe-S cluster-containing proteins, such as aconitase and fumarase, that contain solvent-exposed Fe-S clusters with a marked sensitivity to redox and nitrosative stress (4). Therefore, the possible contribution of Dps to this phenotype was explored by comparing the aconitase activity of the Δ*dps* and Δ*dps*Δ*ric* strains to that of the wild type and Δ*ric* mutant. The results showed that the Δ*dps* mutation caused a 50% reduction in aconitase activity in log phase (Figure 4A), consistent with a role for Dps in maintaining Fe-S cluster status. As expected, a similar effect was observed for the Δ*ric* mutant, although the reduction in activity (30%) was only approximately half as great as that observed for the Δ*dps* mutant (Figure 4A). Surprisingly, the Δ*dps*Δ*ric* mutant exhibited aconitase activity that was higher than that of the corresponding single mutants and similar to that of the wild type (Figure 4A). These aconitase-activity effects were apparent in both the early-log and the post-exponential phase (OD_{600} 0.6 and 2, respectively; Figure 4A and B), suggesting that the phenotype is independent of growth stage (note that *dps* is stationary-phase induced).

Similar effects were observed when testing the activity of another Fe-S enzyme, namely fumarase. The data showed a reduction of 70% in fumarase activity in the Δ*dps* mutant

241 when compared to wild type during the early-log phase (OD_{600}=0.6). Accordingly, in the
242 Δ*ric* mutant there was a reduction in fumarase activity of about 40% while the double
243 mutant Δ*dps*Δ*ric* displayed a fumarase activity similar to that of the wild type (Figure 4C).

244 The restoration of aconitase and fumarase activity to wildtype levels in the double *dps-ric*
245 mutant (with respect to the corresponding single mutants) suggests that the negative impact
246 of the lack of the RIC protein on such activity is dependent on the presence of Dps (and
247 vice-versa), and this in turn indicates a hitherto unrecognised functional interdependence
248 for these two proteins.

249 The association of the above aconitase-activity effects with the RIC protein was confirmed
250 by complementation using a multicopy plasmid bearing the wild type *ric* gene under
251 control of its natural promoter. Complementation of the single Δ*ric* mutant led to the
252 recovery of aconitase activity to levels similar to those of the wild type (Figure 4D). More
253 importantly, provision of a wild type version of *ric* (in multicopy) caused a large (60%) and
254 significant reduction in the aconitase activity of the Δ*dps*Δ*ric* double mutant (Figure 4D).
255 Thus, as anticipated, the *ric*-complemented double mutant exhibited the same phenotype as
256 the *dps* mutant. This confirms that the RIC protein is responsible for decreasing aconitase
257 activity in a dps^- background.

258 To investigate whether the role of the RIC protein in lowering aconitase activity in the *dps*
259 mutant is dependent on a biochemically-functional version of the RIC protein, the ability of
260 a RIC protein variant (lacking a complete di-iron site due to an E133L substitution; (10)),
261 was used in the complementation experiments (Figure 4D). The resulting activity data

clearly show that he non-functional E133L-RIC variant does not enable a notable decrease in aconitase activity when expressed in the Δ*dps*Δ*ric* strain (Figure 4D).

In summary, the above data suggest that in the absence of Dps, the RIC protein has a deleterious effect on aconitase and fumarase activities, but that such an effect is not exhibited when Dps is present. This would imply that the interaction between Dps and the RIC protein, as revealed here, acts to ensure that neither of these two proteins can participate in processes that negatively impact the activity of these Fe-S enzymes.

RIC does not interact with other *E. coli* iron-storage proteins

Escherichia coli Dps is an iron-sequestering protein composed of 12 identical subunits forming a shell surrounding a central cavity where up to ~500 ferric iron atoms can be sequestered. As *E. coli* encodes two other iron-storage proteins, namely bacterioferritin (Bfr) and ferritin (FtnA), the possibility that the RIC protein might interact with these other iron-storage proteins was also investigated. Thus, corresponding BiFC experiments were performed in cells carrying recombinant plasmids that express the RIC protein with either Bfr or FtnA, as N- or C-terminal fusions to GFP domains. The resulting fluorescence intensity data failed to support any protein-protein interaction between the RIC protein and Bfr or FtnA (Figure 5A).

In a second set of experiments, the aconitase activity of wild type, Δ*ric*, Δ*bfr*, Δ*ftnA*, Δ*bfr*Δ*ric* and Δ*ftnA*Δ*ric* strains, grown to the exponential phase (OD_{600} of 0.6), was determined. Similarly to the Δ*dps* strain, the Δ*bfr* and Δ*ftnA* strains both displayed ~50%

lower aconitase activity levels (Figure 5B). But contrary to the effect of combining the Δ*dps* and Δ*ric* mutations, the combined absence of the RIC protein and the Bfr or FtnA proteins resulted in aconitase activities similar to those present in the correspondent single mutant strains (Figure 5B). Thus, the lower aconitase activity caused by the Δ*ric* mutation is not additive with respect to the lower activity resulting from the Δ*bfr* or Δ*ftnA* mutations. Further, it can be concluded that (unlike Dps) Bfr and FtnA do not interact with the RIC protein, and that their absence does not result in a RIC-protein dependent decrease in aconitase activity.

The RIC protein increases intracellular ROS levels when Dps is absent

Dps protects cells from oxidative stress due to its ability to couple the reduction of hydrogen peroxide to water with the oxidation of free-ferrous iron to sequestered-ferric iron. In addition, its association with DNA helps to prevent ROS-induced DNA damage (24). This suggests that the role of Dps in preventing RIC-protein induced inhibition of aconitase activity may arise from the ability of Dps to detoxify ROS that might be produced by the di-iron centre of the RIC protein (e.g. through binding and reduction of oxygen). Therefore, the ROS content of Δ*ric*, Δ*dps* and Δ*dps*Δ*ric* strains were compared with those found in the wild type to determine whether the presence of the RIC protein, in the absence of Dps, results in raised levels of ROS (Figure 6A). Data show that the wild type and Δ*ric* mutant contain similar amounts of ROS while the Δ*dps* strain had significantly higher (~2-fold) levels (Figure 6A). This is as expected given the known role of Dps in redox-stress resistance (24). However, introduction of the *ric* mutation into the *dps* mutant eliminated

the increased intracellular ROS levels of the single Δ*dps* mutant (Figure 6A). This suggests that the raised ROS levels of the *dps* single mutant are a consequence of an increase in RIC-protein-dependent ROS production which thus supports a role for Dps in interacting with the RIC protein to restrict its release of ROS species.

To discover whether other elements of the redox-stress resistance response might also act to lessen RIC-protein induced ROS production, the Δ*ric* mutation was introduced into a strain (Δ*hpx*) lacking capacity to degrade hydrogen peroxide due to inactivation of both catalase genes as well as the alkyl-hydroperoxide reductase genes (Table 1; (25, 26)). Assay of the resulting aconitase activity levels showed that the Δ*hpx*Δ*ric* quadruple mutant has activity levels similar to those determined for the Δ*ric* and Δ*hpx* mutants (Figure 6B). Therefore, we concluded that the three major peroxidases (KatE, KatG, AhpCF) of *E. coli* are not involved in countering any RIC-protein mediated ROS production, at least under conditions where Dps is active.

Discussion

Aconitase and fumarase are enzymes of the TCA cycle that are prone to oxidative stress damage. We previously showed that the di-iron RIC protein repairs these enzymes and is able to transfer iron to Fe-S containing proteins (4–7). In the work described here, we screened an *E. coli* BACTH library in order to identify proteins that interact with the RIC protein and thus might be required to assist its function. As a consequence of our screening, Dps emerged as a RIC protein interaction candidate. This suggested interaction was supported by generation and analysis of additional Dps and RIC protein BACTH constructs

and by GFP complementation and pull-down assays. Dps belongs to the ferritin superfamily which led us to investigate the possible interaction of RIC with the two other ferritins present in *E. coli*, namely ferritin and bacterioferritin. However, none of these proteins were found to interact with the RIC protein or to influence its activity *in vivo*.

We also observed that inactivation of the RIC protein resulted in lower aconitase and fumarase activity, which is consistent with previous findings indicating that this protein contributes to the protection of solvent accessible Fe-S clusters from ROS damage under aerobic growth conditions (6). Similar results were herein obtained for the single mutant strains of *dps*, *ftnA* and *bfr*, indicating that lack of any of these gene products results in lower endogenous aconitase activity. The role of FtnA and Bfr in aconitase protection was previously demonstrated as the two ferritins promote the reactivation of aconitase activity following stress damage in *Salmonella enterica* serovar Typhimurium (27). In contrast with our findings with *E. coli*, no loss of aconitase activity was observed for *S. enterica ftnA* or *bfr* single mutants in the absence of stress; this discrepancy may be related to different physiological roles and expression control of ferritins in *Salmonella* and *E. coli* species (27, 28).

A surprising result was the finding that the defective aconitase activity of the Δ*dps* and Δ*ric* single mutant strains was reversed when these two mutations were combined in the Δ*dps*Δ*ric* double mutant, such that activity was restored to that measured in the wild type. This result, together with the lower amounts of ROS observed in the Δ*dps*Δ*ric* mutant compared to the Δ*dps* mutant, suggests that the RIC protein is responsible for the generation of ROS, but only in the absence of Dps and, thus, that the interaction of Dps and the RIC protein serves to enable Dps to restrict ROS release (which is presumed to damage

the Fe-S cluster of aconitase and fumarase, and hence lower the observed activity of these enzymes in a *dps* mutant) by the RIC protein. Interestingly, other redox-stress resistance components (KatE, KatG and AhpCF) failed to impact the RIC-protein-mediated inhibition of aconitase activity (at least in the presence of Dps). These results suggest that the effect of Dps on the ROS-generation activity of the RIC protein is one that is highly specific and not replicated by the other peroxide-consuming cytosolic factors examined. Indeed, the findings relayed here indicate that a direct interaction is required to enable Dps to quench the ROS-generating activity of the RIC protein. The exact mechanism involved in the apparent quenching of RIC-protein-mediated ROS production by Dps is unclear; such understanding will require *in vitro* reaction studies combining the Dps and RIC proteins. However, two possible processes by which Dps could exert a ROS-quenching action upon the RIC protein can be considered: Dps might sequester iron released from the di-iron site of the RIC protein and thus restrict Fe-driven Fenton chemistry; or Dps could consume hydrogen peroxide (or hydroxyl radicals; (15, 29)) generated by the RIC protein through reaction at its di-iron site with molecular oxygen.

Although the absence of the RIC protein in the presence of Dps resulted in reduced aconitase and fumarase activity, lack of RIC protein had no impact on ROS levels when Dps was present. The reason for this effect is unclear but may indicate a role for the RIC protein in supply of iron from Dps for Fe-S cluster repair and/or synthesis.

The proposed role of the RIC protein (4) is to repair damaged Fe-S clusters of [Fe-S]-proteins, such as aconitase and fumarase, by donating iron from its di-iron centre leading to the formation of an intermediate mononuclear iron centre that is prone to react with oxygen to generate ROS such as hydrogen peroxide. In this process, the interaction with Dps would

373 fulfil two roles, namely by trapping ROS released by the RIC protein and providing a sink
374 for iron liberated from the di-iron centre of RIC.

375 In conclusion, we report an interaction between the Dps and RIC proteins of *E. coli* which
376 represents the first example of a protein that interacts with the ferritin-like Dps protein. In
377 addition, our results indicate that the Dps-RIC protein interaction contributes to the
378 function of RIC, which is one of the few known bacterial proteins involved in repair.

379

380

381

382

Materials and Methods

Bacterial strains and growth conditions

Escherichia coli strains used in this work are listed in Table 1, and were grown at 37 °C. *E. coli* XL2Blue and *E. coli* reporter strain DHM1 non-reverting adenylate cyclase deficient (*cya*) were used as host strain and for detection of protein-protein interactions, respectively.

Construction of the *E. coli* double mutant strains was performed by bacteriophage P1-mediated transduction (30), and the corrected mutations were confirmed by PCR using primers listed in Table 2.

E. coli cells were grown in LB medium under aerobic conditions in flasks containing a 1/5 volume of culture or under anaerobic conditions in rubber seal-capped flasks filled with medium and extensively bubbled with nitrogen prior to growth. For the stress assays, cells were grown, at 37 °C and 150 rpm, in M9B minimal medium (60 mM K_2HPO_4, 33 mM KH_2PO_4, 7.6 mM $(NH_4)_2SO_4$, 1.7 mM sodium citrate, 1 mM $MgSO_4$ and 10 µM $MnCl_2$, pH 7) supplemented with 10 µg/mL thiamine and 40 µg/mL L-arginine, L-leucine, L-proline, L-threonine and 40 mM glucose. Cultures at an OD_{600} of 0.3 were either left untreated or exposed to 4 mM H_2O_2 for 6 h or 250 µM spermine-NONOate for 9 h.

BACTH experiments

The Bacterial Adenylate Cyclase-based Two-Hybrid (BACTH) system assay (17) was used to identify RIC-interacting proteins. *E. coli* RIC protein was fused to the C-terminal of

Bordetella pertussis Cya (adenylate cyclase) T25 domain (pKT25-RIC) and used to screen an *E. coli* MC4100 gene library containing chromosomal fragments fused to the N-terminal of *B. pertussis* Cya T18 domain. The DNA fragments were obtained by partial digestion with *Sau*3AI and cloning into the *Bam*HI site of pUT18 plasmids (18). About 1 µg of pUT18*Bam*HI DNA library was transformed together with pKT25-RIC into *E. coli* DHM1 cells by electroporation. Blue colonies present in Amp^R Cm^R selective plates (L-agar with 5-bromo-4-chloro-3-indolyl β-D-galactopyranoside (X-Gal)) were identified after incubation at 30 ^oC for 36 h, and cells with the highest β-galactosidase were considered to contain recombinant plasmids harbouring genes encoding polypeptides that interact with the *E. coli* RIC protein. Twenty two colonies were obtained and the corresponding plasmids were isolated, co-transformed with pKT25-RIC plasmid in *E. coli* DHM1, and the strength of the protein-protein interactions observed was again estimated by quantification of the β-galactosidase activity. Seven isolates considered positive were named 'A' to 'G' (Figure 1), and sequenced using primer $T18_{Fw}$ (Table 2). To identify the encoded genes, the sequences were screened against the *E. coli* K-12MG1655 genome using BLAST.

Genes coding for the RIC protein and Dps were PCR amplified from *E. coli* K-12 genomic DNA using the oligonucleotides described in Table 2, and cloned into pKT25 (fused to Cya C-terminal T25 domain), pKNT25 (fused to Cya N-terminal T25 domain), pUT18 (fused to Cya N-terminal T18 domain) and pUT18C (fused to Cya C-terminal T18 domain) plasmids, and the enzyme *Pfu* DNA polymerase (Thermo Scientific). The resulting recombinant plasmids encoded Dps or RIC with either a C- or N-terminally linked T25 or T18 domain from the *B. pertussis* Cya protein. Two complementary plasmids, one carrying a T25 fragment and the other a T18 fragment, were co-transformed into the *E. coli* DHM1 strain (*cya*$^-$). *E. coli* DHM1 cells containing the *ric*-encoding pUT18 or pUT18C plasmids

were co-transformed with complementary pKTN25 empty plasmid that served as negative controls.

In all cases, false positives were tested by co-transformation of *E. coli* DHM1 with plasmids containing each gene and pKT25-TorD, which expresses *E. coli* TorD that binds non-specifically to a wide variety of polypeptides (31).

For β-galactosidase activity determination (32), at least 3 representative colonies of each transformation plate were inoculated, in duplicate, in LB medium, and following an overnight growth at 37 ºC, transformant cultures were re-inoculated (at a 0.01 dilution) into LB with ampicillin (100 μg/mL), kanamycin (50 μg/mL) and IPTG (0.5 mM). When cultures reached an OD_{600}=0.5 (approximately after 16 h of growth, at 30 ºC), 1 mL of each culture was collected by centrifugation (5000 *g*, 5 min at 4 ºC). The pellets were lysed by incubation with 100 μL BugBuster HT 1x (Novagen) at 37 ºC, for 30 min. Cellular debris was then removed by centrifugation and the β-galactosidase activities were assayed in 20 μL suspensions in a microplate reader. The assays were initiated by addition of a reaction mixture comprising: 0.27% β-mercaptoethanol (v/v) and 0.9 mg/mL ONPG (o-nitrophenyl-β-D-galactopyranoside) in buffer A (60 mM $Na_2HPO_4.7H_2O$, 40 mM $NaH_2PO_4.H_2O$, 1 mM $MgSO_4.7H_2O$, 10 mM KCl). Reactions were incubated at 28 ºC, and the absorbance was recorded at 420 nm at 2 min intervals, for 90 min. The β-galactosidase specific activity was defined as ONP/min/milligram of protein. Interactions were considered positive for those reactions where β-galactosidase activity was at least four times higher than the negative control.

Bimolecular fluorescence complementation (BiFC) assays

BiFC assay was performed essentially as described previously (33). For this purpose, the genes encoding RIC protein, a truncated version of the RIC protein (lacking the first 57 amino acid residues in N-terminal (10)), Dps, Bfr and FtnA were PCR amplified from genomic DNA of *E. coli* K-12 using the oligonucleotides described in Table 2. Tthe DNA fragments were cloned into vectors (pET11a-link-N-GFP and pMRBAD-link-C-GFP (33)) that express the green fluorescence protein, GFP, to allow formation of corresponding N- or C-terminal GFP fusions, respectively. Cloning was achieved using *Xho*I and *Bam*HI sites (for cloning into pET11a-link-N-GFP) or *Nco*I and *Aat*II sites (for cloning into pMRBAD-link-C-GFP) sites, except for Dps for which *Sph*I replaced *Nco*I. All recombinant plasmids were sequenced confirming the integrity of the genes and the absence of undesired mismatches. Cells harboring pET11a-link-N-GFP and pMRBAD-link-C-GFP served as negative control.

E. coli BL21(DE3)Gold (Agilent) was co-transformed with the resulting recombinant pET11a-link-N-GFP and pMRBAD-link-C-GFP vectors, in various combinations (RIC/Dps, truncated-RIC/Dps, RIC/Bfr and RIC/FtnA), and plated on selective LB-agar. Colonies were inoculated in LB medium, grown overnight, at 37 °C and 150 rpm, and plated onto inducing LB agar medium containing 20 µM IPTG and 0.2% of arabinose. After an overnight incubation at 30 ˚C followed by two days incubation at room temperature, colonies were suspended in PBS and spread onto 1.7% agarose slides. Cells were examined for green fluorescence in a Leica DM6000 B upright microscope coupled to an Andor iXon+ camera, using a 1000x amplification and a FITC filter. The images were analysed using the MetaMorph Microscopy Automation and Image Analysis Software.

Pull-down and Western Blot assays

The genes encoding RIC and Dps were amplified from *E. coli* K-12 genomic DNA by PCR, using the oligonucleotides listed in Table 2, cloned into pET28a and pACYCDuet-1 vectors, respectively, and sequenced which confirmed their integrity and the absence of undesired mutations. *E. coli* BL21(DE3)Gold was transformed with the following pair of plasmids : i) pET28a-RIC (expressing the RIC protein fused to a N-terminal His-Tag-RIC) and pACYCDuet-1-Dps (expressing a non-labelled Dps); and ii) pET28a (empty vector) together with pACYCDuet-1-Dps. Cells harbouring the later pair of recombinant plasmids served as control samples. Cells were grown in LB medium, supplemented with 10 μM of Fe and the appropriate antibiotics, at 30 ˚C to an OD_{600} of 0.3. At this time, 0.3 mM IPTG was added to induce the expression of the His-tagged-RIC and Dps proteins, and after 4 h the cross-linking agent formaldehyde (1% final concentration) was added to the cells. The cross-linking reaction (34) was carried at 37 ˚C for 20 min, and the reaction was stopped by incubation with glycine (final concentration of 0.5 M) at room temperature for 5 min. Bacterial cells were harvested by centrifugation, washed twice with PBS and resuspended in PBS. Cells were disrupted in a French Press (Thermo) and cell debris was removed by centrifugation. The total protein concentration of the supernatants was determined by the Pierce BCA Protein Assay Kit (Thermo Scientific). For the pull-down experiments, these supernatants were loaded into Ni-Chelating Sepharose Fast Flow columns (GE Healthcare), which were first washed with 10 mM Tris-HCl (pH 7.5), and the proteins were eluted with imidazole containing buffers. The protein fractions were analysed by denaturing 12.5% SDS-PAGE, in which the cross-linking promoted by formaldehyde was reversed by heating, and analysed by Western blotting

For Western Blot analysis, samples that were first resolved by SDS-PAGE were transferred to a nitrocellulose blotting membrane (GE Healthcare) in a Trans-blot semi-dry cell apparatus (Bio-Rad). The membrane was blocked by addition of TBS (20 mM Tris-HCl pH 7.5, 500 mM NaCl) containing 5% of dried skimmed milk and incubation at room temperature for 1 h. Then, the membrane was incubated with the primary antibody against *E. coli* K-12 Dps (1:1000 dilution in TBS-T (TBS + 0.05% Tween-20) plus 5% of dried skimmed milk). Following an overnight incubation at 4 ˚C, the membrane was washed with TBS-T and incubated with the secondary antibody (anti-rabbit IgG-alkaline phosphatase from Sigma) diluted 1:10000 in TBS-T + 5% of dried skimmed milk). The reaction proceeded for 1 h at room temperature and the color was developed by addition of 10 μL of NBT-BCIP (Sigma) in 10 mL buffer (100 mM Tris-HCl pH 9.5, 100 mM NaCl, 5 mM $MgCl_2$).

Enzyme activity assays and determination of endogenous ROS

E. coli wild type, Δ*ric*, Δ*dps* and Δ*dps* Δ*ric* strains that were transformed with either pUC18, pUC18-RIC or pUC18-RIC-E133L (prepared described in (10)) were tested for endogenous aconitase and fumarase activities. To this end, the *E. coli* cells strains were grown in LB medium at 37 ºC, under aerobic conditions, to an OD_{600} of 0.6 and 2, as indicated in each case.

For the aconitase assays, cells grown to the desired cell density were centrifuged, washed in reaction buffer (50 mM Tris-HCl, 0.6 mM $MnCl_2$, pH 8), and the pellets were frozen in liquid nitrogen. The following experiments were performed under anaerobic conditions.

Prior to the activity assay, the cell pellets were resuspended in reaction buffer containing 0.5 mg/mL lysozyme and 0.2 mg/mL DNAse and incubated on ice for 10 min, and then centrifuged at 9600 *g* for 10 min, at 4 ^{o}C. The aconitase activity was determined in these supernatants (50 µL) in reaction mixtures that also contained 200 µM $NADP^{+}$, 1 U isocitrate dehydrogenase and 30 mM sodium citrate (10), and by recording the formation of NADPH at 340 nm.

For the fumarase activity assays (35), once the cells reached the desired cell density they were centrifuged, washed with 50 mM sodium phosphate pH 7.3 buffer, and frozen in liquid nitrogen. Cell pellets were resuspended in 2 mL of the same phosphate buffer, lysed by five freeze-thaw cycles that used liquid nitrogen and a water bath at room temperature. The resulting cell extracts were cleared by addition of sodium deoxycholate, to a final concentration of 0.5%. Fumarase activity was determined under anaerobic conditions in reaction mixtures that contained the cell lysates (10 µL) and 50 mM L-malate (which is quickly converted to fumarate) and by following the consumption of fumarate at 240 nm.

Endogenous reactive oxygen species content was determined in *E. coli* wild type, Δ*ric*, Δ*dps*, Δ*dps*Δ*ric*, Δ*bfr*, Δ*bfr*Δ*ric*, Δ*ftnA*, Δ*ftnA*Δ*ric* strains (Table 1). Cells were grown aerobically to an OD_{600} of 0.6, collected by centrifugation, resuspended in PBS, and distributed in 96-well microtitre plates. Following the addition of dichloro-dihydro-fluorescein diacetate (10 µM DCFH-DA), the fluorescence was measured in a spectrofluorimeter Varian Cary (Agilent) at λ_{ex} = 485 nm and λ_{em} = 538 nm,, and for 2 h.

The Fluorescence Intensity (FI) was normalized in relation to the optical density of each culture at 600 nm.

Acknowledgments

We thank Professor Hirotada Mori (Graduate School of Biological Sciences, Nara Institute of Science and Technology, Ikoma, Nara, Japan) for provision of the mutants from the Keio collection, and Professor James Imlay (Department of Microbiology, B103 CLSL, 601 S Goodwin Ave, Urbana, IL 61801, USA) for the Hpx mutant. We also grateful to Professor Tracy Palmer and Frank Sargent (Centre for Bacterial Cell Biology, Newcastle University) for providing the BACTH *E. coli* library.

This work was financially supported by: Project LISBOA-01-0145-FEDER-007660 (Microbiologia Molecular, Estrutural e Celular) funded by FEDER funds through COMPETE2020 - Programa Operacional Competitividade e Internacionalização (POCI) and by national funds through FCT - Fundação para a Ciência e a Tecnologia" for grants PTDC/BBB-BQB/5069/2014, and SFRH/BD/118545/2016 (LSOS). This project has also received funding from the European Union's Horizon 2020 research and innovation programme under grant agreement number 810856.

References

1. Overton TW, Justino MC, Li Y, Baptista JM, Melo AMP, Cole J a, Saraiva LM. 2008. Widespread distribution in pathogenic bacteria of di-iron proteins that repair oxidative and nitrosative damage to iron-sulfur centers. J Bacteriol 190:2004–2013.

2. Chow ED, Liu OW, O'Brien S, Madhani HD. 2007. Exploration of whole-genome responses of the human AIDS-associated yeast pathogen *Cryptococcus neoformans* var grubii: nitric oxide stress and body temperature. Curr Genet 52:137–148.

3. Harrington JC, Wong SMS, Rosadini C V., Garifulin O, Boyartchuk V, Akerley BJ. 2009. Resistance of *Haemophilus influenzae* to reactive nitrogen donors and gamma interferon-stimulated macrophages requires the formate-dependent nitrite reductase regulator-activated ytfE gene. Infect Immun 77:1945–1958.

4. Justino MC, Almeida CC, Teixeira M, Saraiva LM. 2007. *Escherichia coli* di-iron YtfE protein is necessary for the repair of stress-damaged iron-sulfur clusters. J Biol Chem 282:10352–10359.

5. Balasiny B, Rolfe MD, Vine C, Bradley C, Green J, Cole J. 2018. Release of nitric oxide by the *Escherichia coli* YtfE (RIC) protein and its reduction by the hybrid cluster protein in an integrated pathway to minimize cytoplasmic nitrosative stress. Microbiology 164:563–575.

6. Justino MC, Almeida CC, Gonçalves VL, Teixeira M, Saraiva LM. 2006. *Escherichia coli* YtfE is a di-iron protein with an important function in assembly of iron-sulphur clusters. FEMS Microbiol Lett 257:278–284.

580 7. Nobre LS, Garcia-Serres R, Todorovic S, Hildebrandt P, Teixeira M, Latour J-M,
581 Saraiva LM. 2014. *Escherichia coli* RIC is able to donate iron to iron-sulfur clusters.
582 PLoS One 9:e95222.

583 8. Silva LO, Nobre LS, Mil-Homens D, Fialho A, Saraiva LM. 2018. Repair of Iron
584 Centers RIC protein contributes to the virulence of *Staphylococcus aureus*.
585 Virulence 9:312–317.

586 9. Todorovic S, Justino MC, Wellenreuther G, Hildebrandt P, Murgida DH, Meyer-
587 Klaucke W, Saraiva LM. 2008. Iron-sulfur repair YtfE protein from *Escherichia*
588 *coli*: Structural characterization of the di-iron center. J Biol Inorg Chem 13:765–770.

589 10. Nobre LS, Lousa D, Pacheco I, Soares CM, Teixeira M, Saraiva LM. 2015. Insights
590 into the structure of the diiron site of RIC from *Escherichia coli*. FEBS Lett
591 589:426–431.

592 11. Lo F-C, Hsieh C-C, Maestre-Reyna M, Chen C-Y, Ko T-P, Horng Y-C, Lai Y-C,
593 Chiang Y-W, Chou C-M, Chiang C-H, Huang W-N, Lin Y-H, Bohle DS, Liaw W-F.
594 2016. Crystal Structure Analysis of the Repair of Iron Centers Protein YtfE and Its
595 Interaction with NO. Chem - A Eur J:1–10.

596 12. Almiron M, Link a J, Furlong D, Kolter R. 1992. A novel DNA-binding protein
597 with regulatory and protective roles in starved *Escherichia coli*. Genes Dev 6:2646–
598 2654.

599 13. Grant R a, Filman DJ, Finkel SE, Kolter R, Hogle JM. 1998. The crystal structure of
600 Dps, a ferritin homolog that binds and protects DNA. Nat Struct Biol 5:294–303.

601 14. Calhoun LN, Kwon YM. 2011. Structure, function and regulation of the DNA-

602 binding protein Dps and its role in acid and oxidative stress resistance in *Escherichia*
603 *coli*: a review. J Appl Microbiol 110:375–386.

604 15. Zhao G, Ceci P, Ilari A, Giangiacomo L, Laue TM, Chiancone E, Chasteen ND.
605 2002. Iron and hydrogen peroxide detoxification properties of DNA-binding protein
606 from starved cells. A ferritin-like DNA-binding protein of *Escherichia coli*. J Biol
607 Chem 277:27689–27696.

608 16. Karas VO, Westerlaken I, Meyer AS. 2015. The DNA-Binding protein from starved
609 cells (Dps) utilizes dual functions to defend dells against multiple stresses. J
610 Bacteriol 197:3206–3215.

611 17. Karimova G, Pidoux J, Ullmann A, Ladant D. 1998. A bacterial two-hybrid system
612 based on a reconstituted signal transduction pathway. Proc Natl Acad Sci U S A
613 95:5752–5756.

614 18. Jack RL, Buchanan G, Dubini A, Hatzixanthis K, Palmer T, Sargent F. 2004.
615 Coordinating assembly and export of complex bacterial proteins. EMBO J 23:3962–
616 3972.

617 19. Blaha G, Stanley RE, Steitz TA. 2009. Formation of the first peptide bond: The
618 structure of EF-P bound to the 70S ribosome. Science 325:966–970.

619 20. Ganoza MC, Aoki H. 2000. Peptide bond synthesis: function of the *efp* gene product.
620 Biol Chem 381:553–559.

621 21. Bishop RE, Leskiw BK, Hodges RS, Kay CM, Weiner JH. 1998. The entericidin
622 locus of *Escherichia coli* and its implications for programmed bacterial cell death. J
623 Mol Biol 280:583–596.

624 22. Livshits VA, Zakataeva NP, Aleshin V V., Vitushkina M V. 2003. Identification and
625 characterization of the new gene *rhtA* involved in threonine and homoserine efflux in
626 *Escherichia coli.* Res Microbiol 154:123–135.

627 23. Magliery TJ, Wilson CGM, Pan W, Mishler D, Ghosh I, Hamilton AD, Regan L.
628 2005. Detecting protein-protein interactions with a green fluorescent protein
629 fragment reassembly trap: scope and mechanism. J Am Chem Soc 127:146–157.

630 24. Chiancone E, Ceci P. 2010. The multifaceted capacity of Dps proteins to combat
631 bacterial stress conditions: Detoxification of iron and hydrogen peroxide and DNA
632 binding. Biochim Biophys Acta 1800:798–805.

633 25. Park S, You X, Imlay J a. 2005. Substantial DNA damage from submicromolar
634 intracellular hydrogen peroxide detected in Hpx- mutants of *Escherichia coli*. Proc
635 Natl Acad Sci U S A 102:9317–9322.

636 26. Seaver LC, Imlay JA. 2004. Are respiratory enzymes the primary sources of
637 intracellular hydrogen peroxide? J Biol Chem 279:48742–48750.

638 27. Velayudhan J, Castor M, Richardson A, Main-Hester KL, Fang FC. 2007. The role
639 of ferritins in the physiology of *Salmonella enterica* sv. Typhimurium: A unique role
640 for ferritin B in iron-sulphur cluster repair and virulence. Mol Microbiol 63:1495–
641 1507.

642 28. Abdul-Tehrani H, Hudson AJ, Chang YS, Timms AR, Hawkins C, Williams JM,
643 Harrison PM, Guest JR, Andrews SC. 1999. Ferritin mutants of *Escherichia coli* are
644 iron deficient and growth impaired, and fur mutants are iron deficient. J Bacteriol
645 181:1415–1428.

29. Bellapadrona G, Ardini M, Ceci P, Stefanini S, Chiancone E. 2010. Dps proteins prevent Fenton-mediated oxidative damage by trapping hydroxyl radicals within the protein shell. Free Radic Biol Med 48:292–297.

30. Lennox ES. 1955. Transduction of linked genetic characters of the host by bacteriophage P1. Virology 1:190–206.

31. Pommier J, Mejean V, Giordano G, Iobbi-Nivol C. 1998. TorD, a cytoplasmic chaperone that interats with the unfolded trimethylamine N-oxide reductase enzyme (TorA) in *Escherichia coli.* J Biol Chem 273:16615–16620.

32. Thibodeau SA, Fang R, Joung JK. 2004. High-throughput B-galactosidase assay for bacterial cell-based reporter systems. Biotechniques 36:410–415.

33. Wilson CGM, Magliery TJ, Regan L. 2004. Detecting protein-protein interactions with GFP-fragment reassembly. Nat Methods 1:255–262.

34. Ferreira E, Giménez R, Aguilera L, Guzmán K, Aguilar J, Badia J, Baldomà L. 2013. Protein interaction studies point to new functions for *Escherichia coli* glyceraldehyde-3-phosphate dehydrogenase. Res Microbiol 164:145–154.

35. Puchegger S, Redl B, Stoffler G. 1990. Purification and properties of a thermostable fumarate hydratase from the archaeobacterium *Sulfolobus solfataricus*. J Gen Microbiol 136:1537–1541.

36. Vine CE, Justino MC, Saraiva LM, Cole J. 2010. Detection by whole genome microarrays of a spontaneous 126-gene deletion during construction of a *ytf*E mutant: confirmation that a *ytfE* mutation results in loss of repair of iron-sulfur centres in proteins damaged by oxidative or nitrosative stress. J Microbiol Methods

668 81:77–79.

669 37. Baba T, Ara T, Hasegawa M, Takai Y, Okumura Y, Baba M, Datsenko KA, Tomita
670 M, Wanner BL, Mori H. 2006. Construction of *Escherichia coli* K-12 in-frame,
671 single-gene knockout mutants: the Keio collection. Mol Syst Biol 2:1-11

672 38. Seaver LC, Imlay JA. 2001. Alkyl hydroperoxide reductase is the primary scavenger
673 of endogenous hydrogen peroxide in *Escherichia coli*. J Bacteriol 183:7173–7181.

674 39. Jang S, Imlay J a. 2010. Hydrogen peroxide inactivates the *Escherichia coli* Isc iron-
675 sulphur assembly system, and OxyR induces the Suf system to compensate. Mol
676 Microbiol 78:1448–1467.

677

678

679 **Table 1 –Strains and plasmids used in this study**

E.coli	Description	Source
Strains		
DHM1	F′, *cya-854, recA1, endA1, gyrA96* (Nal^R), *thi1, hsdR17, spoT1, rfbD1, glnV44(AS)*	Euromedex
Wild type	K-12 ATCC 23716	ATCC
Δ*ric*	K-12 Δ*ric*::*cat*	(36)
Δ*dps*	JS091 Δ*dps*::*kan*	(37)
Δ*bfr*	JW3298 Δ*bfr*::*kan*	(37)
Δ*ftnA*	MC4100 Δ*ftnA*::*spc*	(28)
Δ*dps*Δ*ric*	K-12 Δ*dps*::*kan*, Δ*ric*::*cat*	This study
Δ*bfr*Δ*ric*	K-12 Δ*bfr*::*kan*, Δ*ric*::*cat*	This study
Δ*ftnA*Δ*ric*	K-12 Δ*ftnA*::*spc*, Δ*ric*::*cat*	This study
MG1655	F^- WT	(38)
SJ90	BW25113 Δ*ric*::*cat*	(39)
LC106 (*hpx*)	Δ*ahpCF'kan*::*'ahpḞ*, Δ(*katG17*::Tn*10*)1, Δ(*katE12*::Tn*10*)1	(26)
Δ*hpx*Δ*ric*	LC106 Δ*ric1*::cat	This study
XL2 Blue	*recA1, endA1, gyrA96, thi-1, hsdR17, supE44, relA1, lac* [F' *proAB*$^+$, *lacIqZ*ΔM15 Tn*10* (Tet^r)]	Agilent
BL21Gold(DE3)	*E. coli* B, F^-, *ompT, hsdS* (r_B^- m_B^-), *dcm*$^+$, Tet^r, *gal*, *λ*(DE3), *endA*, Hte	Agilent

Plasmids		
pUT18/pUT18C	Vector that allows construction of in-frame fusions at the N-terminus/C-terminus of T18 fragment (amino acids 225-399 of CyaA)	(17)
pKT25/pKNT25	Vector that allows construction of in-frame fusions at the N-terminus/C-terminus of T25 fragment (amino acids 1-224 of CyaA)	(17)
pUT18/pUT18C-RIC	RIC fused to T18 fragment in N/C-terminal	This study
pKT25/pKNT25-RIC	RIC fused to T25 fragment in N/C-terminal	This study
pUT18/pUT18C-Dps	Dps fused to T18 fragment in N/C-terminal	This study
pKT25/pKNT25-Dps	Dps fused to T25 fragment in N/C-terminal	This study
pUT18-Zip	Leucine zipper fused to T18 fragment in the N-terminal	(17)
pKT25-Zip	Leucine zipper fused to T25 fragment in the C-terminal	(17)
pUT18-TorD	TorD fused to T18 fragment in N-terminal	(18)
pKT25-TorD	TorD fused to T25 fragment in C-terminal	(18)
*Bam*HI	pUT18 plasmid that contains chromosomal fragments obtained by partial digest of the MC4100 chromosomal DNA with Sau3A1 and cloned into de *Bam*HI site	(18)
pUC18	Expression vector	ATCC

pUC18-RIC	Vector for expression of RIC	(4)
pUC18-RIC-Glu133Leu	Vector for expression of RIC-Glu133Leu	(10)
pET11a-link-GFP	Vector for expression of fusions with N-terminal fragment of GFP	(33)
pMRBAD-link-GFP	Vector for expression of fusions with C- terminal fragment of GFP	(33)
pET11a-RIC-GFP	RIC fused to N-terminal GFP fragment	This study
pMRBAD-RIC-GFP	RIC fused to C-terminal GFP fragment	This study
pET11a-Dps-GFP	Dps fused to N-terminal GFP fragment	This study
pMRBAD-Dps-GFP	Dps fused to C-terminal GFP fragment	This study
pET11a-Bfr-GFP	Bfr fused to N-terminal GFP fragment	This study
pMRBAD-Bfr-GFP	Bfr fused to C-terminal GFP fragment	This study
pET11a-FtnA-GFP	FtnA fused to N-terminal GFP fragment	This study
pMRBAD-FtnA-GFP	FtnA fused to C-terminal GFP fragment	This study
pET11a-RICTrunc-GFP	Truncated RIC fused to N-terminal GFP fragment	This study
pMRBAD-RICTrunc-GFP	Truncated RIC fused to C-terminal GFP fragment	This study
pET-28a	Expression vector	Novagen
pET-28a-RIC(HisTag)	Vector for expression of N-terminal Poly-HisTag-RIC	This study
pACYCDuet-1-Dps	Vector for expression of Dps	This study

680

681 **Table 2 – Oligonucleotides used in this study**

Primer Name	Sequence
Construction of plasmids used in BACTH	
ric_Fw	GAGGTGTCGACTATGGCTTATC
ric_Rv	CTTTTAGGATCCTCACCCGCC
dps_Fw	GTTAATTACTGGGATCCAACATCAAGAGG
dps_Rv	TCCTGTCAGGTACCCGCTTTTATC
T18_Fw	CATTAGGCACCCCAGGCTTTAC
T18_Rv	GAGCGATTTTCCACAACAAGTC
T18C_Fw	CATACGGCGTGGCGGGGAAAAG
T18C_Rv	AGCGGGTGTTGGCGGGTGTCG
T25_Fw	ATGCCGCCGGTATTCCACTG
T25_Rv	CGGGCCTCTTCGCTATTACG
NT25_Fw	CACCCCAGGCTTTACACTTTATGC
NT25_Rv	CAATGTGGCGTTTTTTTCCTTCG
Construction of plasmids used in BiFC	
ric_xhoFw	GAATGAGGTCTCGAGTATGGCTTATC
ric_bamRv	GCGCAATGGGATCCAGCTTTTAGA
ric_ncoFw	GAGGTATCAGCCATGGCTTATCG
ric_aatRv	CCAGCTTTTAGACGTCTCACCC
dps_xhoFw	CGTTAATTACTCGAGCATAACATCAAG
dps_bamRv	GTACTAAGGATCCGCACCATCAGC

dps_sphFw	CAAGAGGATATGCATGCATGAGTACCGCTA
dps_aatRv	CATCAGCGATGGGACGTCTCGATGTTAG
bfr_xhoFw	GAGTGGAAGCGCTCGAGTCAAAAAATG
bfr_bamRv	GGAGGGTTCTGGATCCCGACACG
bfr_ncoFw	GAAGGAGTCAAACCATGGAAGGTGATAC
bfr_aatRv	CGGACGTCCCTTCTTCGCGGATC
truncric_xhoFw	CTTTAAGAAGGCTCGAGACATATGGCTG
truncric_ncoFw	GGAGATATACCCATGGCTGAACAAC
ftna_xhoFw	CAAATATAACCTTTCTCGAGCACTATC
ftna_bamRv	TGAAACGGATCCAGTAAACCTGC
ftna_ncoFw	GAGCACTACCATGGTGAAACCAGAAAT
ftna_aatRv	CGGAGAGGACGTCTTTTGTGTGTC
Construction of plasmids used for protein expression	
pric_ndeFw	AAGAATGAGGTATCACATATGGCTTATCGC
pric_ecoriRv	GGCTGTTTATTGGTAAGAATTCGGCTGCTG
pdps_ndeFw	GAGGATATGAACATATGAGTACCGC
pdps_kpnRV	GTACTAAAGTTCGGTACCATCAGCG
Double mutant construction confirmation	
Conf_dps_Fw	CAGAATAGCGGAACACATAGC
Conf_dps_Rv	GATGCACTAAATAAGTGCGTTG
Conf_bfr_Fw	CTCTTCAAAGAGTGGAAGCG
Conf_bfr_Rv	GATCTCTTATTAACCGGGAGG
Conf_ftnA_Fw	CAAATTATAGTGACGCCACAG

Conf_ftnA_Rv	ACCGATCAGAGTAAGATTTGC
Conf_ric_Fw	AAGAATGAGGTATCACATATGGCTTATCGC
Conf_ric_Rv	GGCTGTTTATTGGTAAGAATTCGGCTGCTG

682

683

Figure Legend

Figure 1: *E. coli* RIC interactions investigated by BACTH. β-Galactosidase activities of *E. coli* DHM1 cell lysates expressing, separately, plasmids A to G, which were extracted from the *Bam*HI library and co-transformed with the pKTN25-RIC (grey bars), pKTN25 empty plasmid (white bars), and pKTN25 fused to TorD (black bars). Each bar represents the mean value ± standard error from results of at least three independent cultures.

Figure 2: *E. coli* RIC interacts with Dps.

A) Bacterial two-hybrid assay: the interaction of the RIC protein, linked to the C- (white bar) or N-terminus (grey bar) of the T18-Cya domain and expressed from pUT18 or pUT18C, respectively, was evaluated in *E. coli* DHM1 co-transformed with pKTN25 containing a Dps linked to the N-terminus of the T25-Cya domain. *E. coli* cells harbouring simultaneously empty pKTN25 and pUT18/pUT18C vectors expressing *ric* fusions served as negative controls (black bars).

B-C) BiFC assays. Cells were co-transformed with vectors expressing either $RIC^{C\text{-}GFP}$ (pMRBAD-link-C-GFP-RIC) or $RIC\text{-}Truncated^{C\text{-}GFP}$ (pMRBAD-link-C-GFP-RICTrunc) with $Dps^{N\text{-}GFP}$ (pET11a-link-N-GFP-Dps). The inverse configurations were also included. **B)** Cells expressing $RIC^{C\text{-}GFP}$ and $Dps^{N\text{-}GFP}$ were analysed by light microscopy (bright field, left upper panel) and fluorescence microscopy (right upper panel). Lower panels depict images of cells co-transformed cells with empty vectors. Images were acquired using a 100x objective and a FITC filter was used for the acquisition of the fluorescence images. **C)** Fluorescence quantification was performed using MetaMorph Microscopy Automation and

Image Analysis Software. Fluorescence values for negative control (empty plasmid vectors) were normalized to 1.

D) Pull-down assays. Lane 1: Cells expressing pET28a-RIC (RIC protein linked to a N-terminal His-Tag-RIC (~30 KDa)) and pACYCDuet-1-Dps (non-labelled Dps (~18 KDa)). Lane 2: Cells expressing pET28a (empty vector) and pACYCDuet-1-Dps (non-labelled Dps (~18 KDa)). Protein fractions were eluted from the Ni-chelating column at 100 mM imidazole and analysed by SDS-PAGE (upper panel) and Western blotting using the anti-*E. coli* Dps antibody (bottom panel).

Values are means ± standard error of at least three independent cultures analysed in duplicate ***p<0.0005 (One-way ANOVA multiple comparison test).

Figure 3: Growth of *E. coli* Δ*ric*, Δ*dps* and Δ*dps*Δ*ric* strains under nitrosative and oxidative stress. *E. coli* wild type, Δ*ric*, Δ*dps* and Δ*dps*Δ*ric* strain were grown under anaerobic **(A)** and aerobic **(B)** conditions. At OD_{600}=0.3, cells were left untreated (white bars), treated (grey bars) with 250 µM spermine NONOate for 7 h **(A)**, or treated with 4 mM H_2O_2 for 5 h **(B)**. Error bars are ± SD for experiments carried out at least three times.

Figure 4: Aconitase and fumarase activity of *E. coli* Δ*ric* and Δ*dps* mutant strains. Aconitase activity of *E. coli* wild type, Δ*ric*, Δ*dps* and Δ*dps*Δ*ric* strains grown aerobically to OD_{600} of 0.6 **(A, D)** or 2.0 **(B)**. Fumarase activity of *E. coli* wild type, Δ*ric*, Δ*dps* and Δ*dps*Δ*ric* strains grown aerobically to OD_{600} of 0.6 **(C).** Complementation experiments of aconitase activity (D) were performed using Δ*ric* and Δ*dps*Δ*ric* strains transformed with

pUC18, and with pUC18 encoding the RIC protein and the mutated Glu133Leu-RIC (a RIC protein where glutamate 133 was site-directed mutated by leucine (10)). Values are represented as normalized to the aconitase or fumarase activity of wild type cells. Values are means (± standard error) of at least two independent cultures analysed in duplicate. *p<0.05; **p<0.005; ns: not significant (unpaired Student's t-test).

Figure 5: Iron-storage proteins Bfr and FtnA do not interact with RIC.

A) The possible interaction between RIC and Bfr and FtnA was analysed by fluorescence microscopy and quantified by MetaMorph Microscopy Automation and Image Analysis Software. Cells were co-transformed with vectors expressing $RIC^{C\text{-}GFP}$ (pMRBAD-C-GFP-RIC) and $Bfr^{N\text{-}GFP}$ (pET11a- N-GFP-Bfr) or $FtnA^{N\text{-}GFP}$ (pET11a-N-GFP-FtnA). The inverse conformations were also examined. Fluorescence values for negative control (empty plasmid vectors) were normalized to 1. Values are means ± standard error of at least three independent cultures analysed in duplicate. ns: not significant (One-way ANOVA multiple comparison test).

B) *E. coli* cells of single (Δ*ric*, Δ*bfr*, Δ*ftnA*) and double mutant strains (Δ*bfr*Δ*ric*, Δ*ftnA*Δ*ric*) were grown aerobically, collected at OD of 0.6 and the aconitase activity was determined. Values are represented as normalized to the aconitase activity of wild type cells. Values are means ± standard error of at least two independent cultures analysed in duplicate. *p<0.05; ns: not significant (unpaired Student's t-test).

Figure 6: Intracellular ROS content of Δ*dps* and Δ*ric* mutant strains, and the effect of combining the Δ*hpx* and Δ*ric* mutations on aconitase activity.

A) The *E. coli* wild type and isogenic Δ*ric*, Δ*dps* and Δ*dps*Δ*ric* mutant strains were grown to OD_{600} of 0.6, and the intracellular ROS levels were measured by incubation of cell suspensions with 10 µM DCFH-DA for 2 h. Fluorescence intensity was normalized according to the final OD (FI/OD).

B) Aconitase activity of the *E. coli* wild type, Δ*ric*, Δ*hpx* (Δ*ahpCF*Δ*katE*Δ*katG*), and Δ*hpx*Δ*ric* strains grown aerobically to the log phase (OD_{600}=0.6). Values are represented as normalized to the aconitase activity of wild type cells.

Values are means (± standard error) of at least two independent cultures analysed in duplicate. ***p<0.0005; ns: not significant (unpaired Student's t-test).

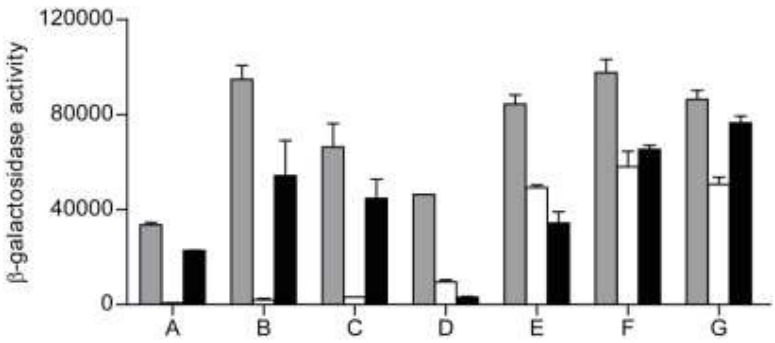

Figure 1: *E. coli* RIC interactions investigated by BACTH. β-Galactosidase activities of *E. coli* DHM1 cell lysates expressing, separately, plasmids A to G, which were extracted from the *Bam*HI library and co-transformed with the pKTN25-RIC (grey bars), pKTN25 empty plasmid (white bars), and pKTN25 fused to TorD (black bars). Each bar represents the mean value ± standard error from results of at least three independent cultures.

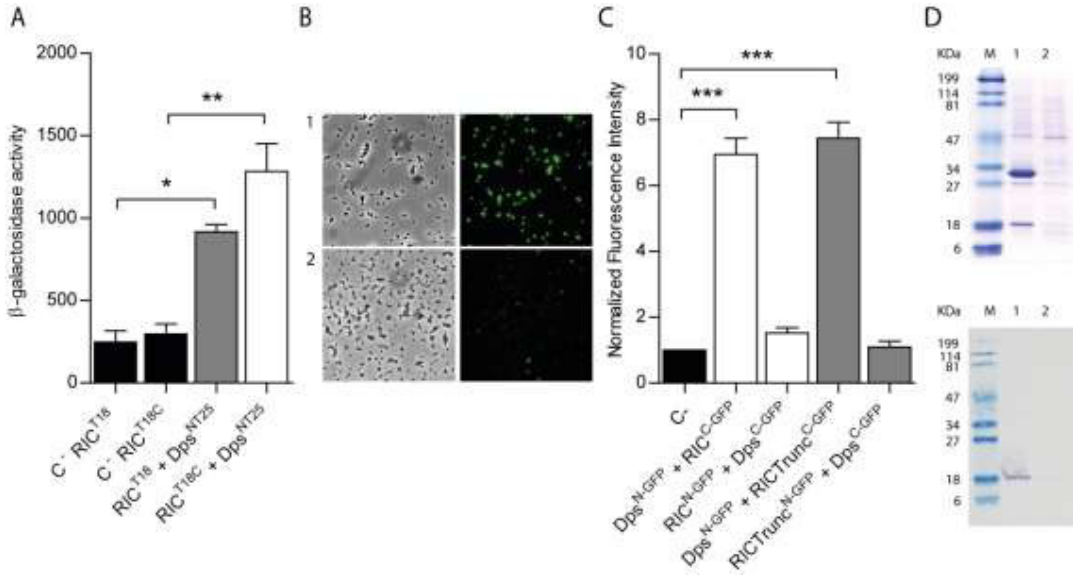

Figure 2: *E. coli* RIC interacts with Dps.

A) Bacterial two-hybrid assay: the interaction of the RIC protein, linked to the C- (white bar) or N-terminus (grey bar) of the T18-Cya domain and expressed from pUT18 or pUT18C, respectively, was evaluated in *E. coli* DHM1 co-transformed with pKTN25 containing a Dps linked to the N-terminus of the T25-Cya domain. *E. coli* cells harbouring simultaneously empty pKTN25 and pUT18/pUT18C vectors expressing *ric* fusions served as negative controls (black bars).

B-C) BiFC assays. Cells were co-transformed with vectors expressing either $RIC^{C\text{-}GFP}$ (pMRBAD-link-C-GFP-RIC) or RIC-$Truncated^{C\text{-}GFP}$ (pMRBAD-link-C-GFP-RICTrunc) with $Dps^{N\text{-}GFP}$ (pET11a-link-N-GFP-Dps). The inverse configurations were also included. **B)** Cells expressing $RIC^{C\text{-}GFP}$ and $Dps^{N\text{-}GFP}$ were analysed by light microscopy (bright field, left upper panel) and fluorescence microscopy (right upper panel). Lower panels depict images of cells co-transformed cells with empty vectors. Images were acquired using a 100x objective and a FITC filter was used for the acquisition of the fluorescence images. **C)** Fluorescence quantification was performed

using MetaMorph Microscopy Automation and Image Analysis Software. Fluorescence values for negative control (empty plasmid vectors) were normalized to 1.

D) Pull-down assays. Lane 1: Cells expressing pET28a-RIC (RIC protein linked to a N-terminal His-Tag-RIC (~30 KDa)) and pACYCDuet-1-Dps (non-labelled Dps (~18 KDa)). Lane 2: Cells expressing pET28a (empty vector) and pACYCDuet-1-Dps (non-labelled Dps (~18 KDa)). Protein fractions were eluted from the Ni-chelating column at 100 mM imidazole and analysed by SDS-PAGE (upper panel) and Western blotting using the anti-*E. coli* Dps antibody (bottom panel).

Values are means ± standard error of at least three independent cultures analysed in duplicate ***$p<0.0005$ (One-way ANOVA multiple comparison test).

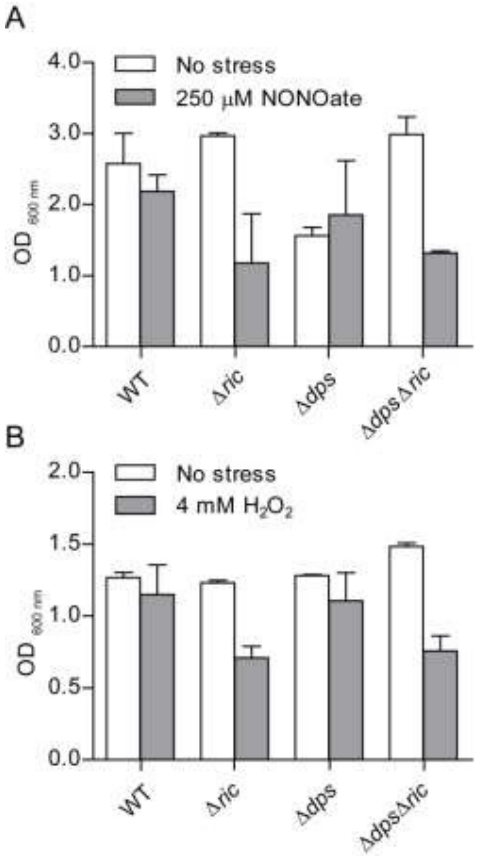

Figure 3: Growth of *E. coli* Δ*ric*, Δ*dps* and Δ*dps*Δ*ric* strains under nitrosative and oxidative stress. *E. coli* wild type, Δ*ric*, Δ*dps* and Δ*dps*Δ*ric* strain were grown under anaerobic **(A)** and aerobic **(B)** conditions. At OD_{600}=0.3, cells were left untreated (white bars), treated (grey bars) with 250 µM spermine NONOate for 7 h **(A)**, or treated with 4 mM H_2O_2 for 5 h **(B)**. Error bars are ± SD for experiments carried out at least three times.

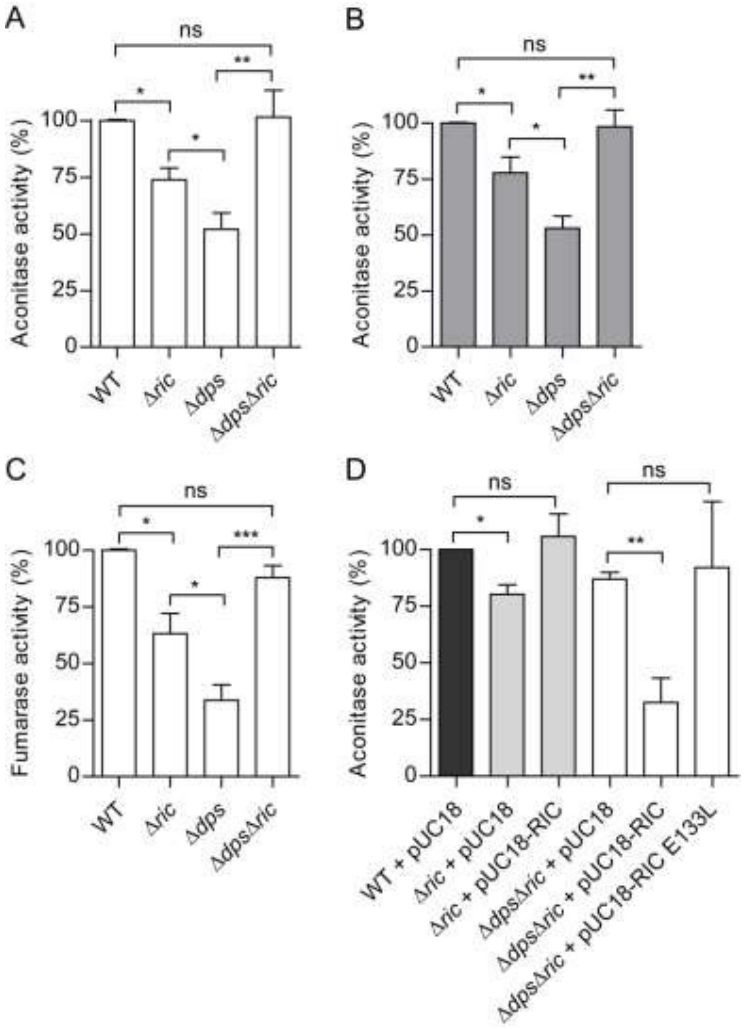

Figure 4: Aconitase and fumarase activity of *E. coli* Δ*ric* and Δ*dps* mutant strains. Aconitase activity of *E. coli* wild type, Δ*ric*, Δ*dps* and Δ*dps*Δ*ric* strains grown aerobically to OD_{600} of 0.6 **(A, D)** or 2.0 **(B)**. Fumarase activity of *E. coli* wild type, Δ*ric*, Δ*dps* and Δ*dps*Δ*ric* strains grown aerobically to OD_{600} of 0.6 **(C).** Complementation experiments of aconitase activity (D) were performed using Δ*ric* and Δ*dps*Δ*ric* strains transformed with pUC18, and with pUC18 encoding the RIC protein and the mutated Glu133Leu-RIC (a RIC protein where glutamate 133 was site-directed mutated by leucine (9)). Values are represented as normalized to the aconitase or fumarase activity of wild type cells. Values are means (± standard error) of at least two

independent cultures analysed in duplicate. *$p<0.05$; **$p<0.005$; ns: not significant (unpaired Student's t-test).

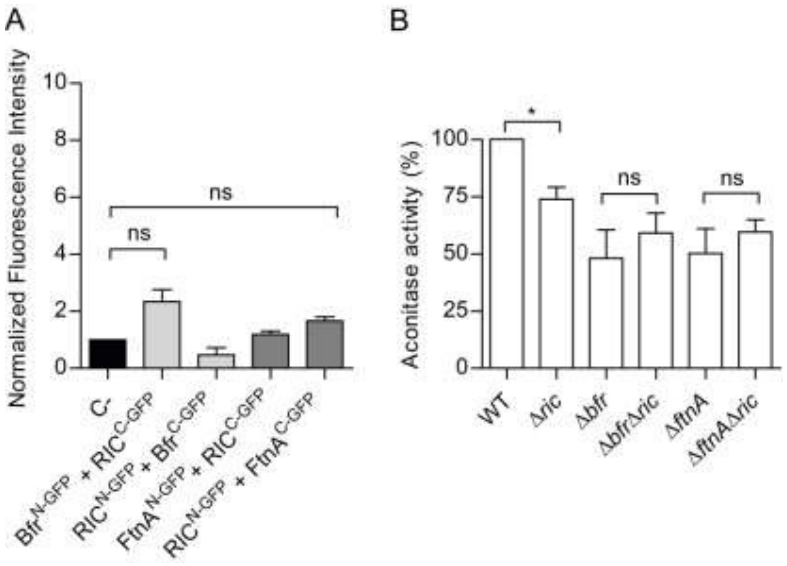

Figure 5: Iron-storage proteins Bfr and FtnA do not interact with RIC.

A) The possible interaction between RIC and Bfr and FtnA was analysed by fluorescence microscopy and quantified by MetaMorph Microscopy Automation and Image Analysis Software. Cells were co-transformed with vectors expressing $RIC^{C\text{-}GFP}$ (pMRBAD-C-GFP-RIC) and $Bfr^{N\text{-}GFP}$ (pET11a- N-GFP-Bfr) or $FtnA^{N\text{-}GFP}$ (pET11a-N-GFP-FtnA). The inverse conformations were also examined. Fluorescence values for negative control (empty plasmid vectors) were normalized to 1. Values are means ± standard error of at least three independent cultures analysed in duplicate. ns: not significant (One-way ANOVA multiple comparison test).

B) *E. coli* cells of single (Δ*ric*, Δ*bfr*, Δ*ftnA*) and double mutant strains (Δ*bfr*Δ*ric*, Δ*ftnA*Δ*ric*) were grown aerobically, collected at OD of 0.6 and the aconitase activity was determined. Values are represented as normalized to the aconitase activity of wild type cells. Values are means ± standard error of at least two independent cultures analysed in duplicate. *$p<0.05$; ns: not significant (unpaired Student's t-test).

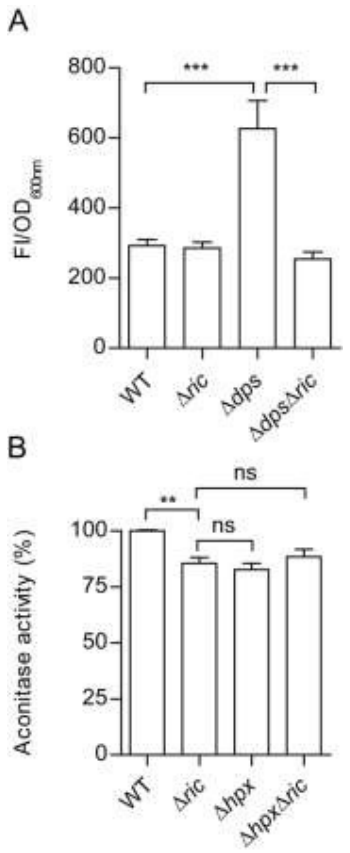

Figure 6: Intracellular ROS content of Δ*dps* and Δ*ric* mutant strains, and the effect of combining the Δ*hpx* and Δ*ric* mutations on aconitase activity.

A) The *E. coli* wild type and isogenic Δ*ric*, Δ*dps* and Δ*dps*Δ*ric* mutant strains were grown to OD_{600} of 0.6, and the intracellular ROS levels were measured by incubation of cell suspensions with 10 µM DCFH-DA for 2 h. Fluorescence intensity was normalized according to the final OD (FI/OD).

B) Aconitase activity of the *E. coli* wild type, Δ*ric*, Δ*hpx* (Δ*ahpCF*Δ*katE*Δ*katG*), and Δ*hpx*Δ*ric* strains grown aerobically to the log phase (OD_{600}=0.6). Values are represented as normalized to the aconitase activity of wild type cells.

Values are means (± standard error) of at least two independent cultures analysed in duplicate. ***$p<0.0005$; ns: not significant (unpaired Student's t-test).